Published in final edited form as:
J Immunol. 2013 February 1; 190(3): 1094–1102. doi:10.4049/jimmunol.1202639.

Focal Adhesion Kinase Regulates the Localization and Retention of Pro-B Cells in Bone Marrow Microenvironments

Shin-Young Park[1], **Peter Wolfram**[1], **Kimberly Canty**[1], **Brendan Harley**[1], **César Nombela-Arrieta**[1], **Gregory Pivarnik**[1], **John Manis**[1], **Hilary E Beggs**[2], and **Leslie E Silberstein**[1]

[1]Transfusion Medicine, Children's Hospital Boston, Harvard Medical School, Boston, Massachusetts 02115, USA

[2]Ophthalmology & Physiology, University of California at San Francisco, San Francisco, California 94143, USA

Abstract

Progenitor B cells reside in complex bone marrow microenvironments where they receive signals for growth and maturation. We reported previously that the CXCL12-FAK-VLA4 pathway plays an important role in progenitor B cell adhesion and migration. Here we have conditionally targeted in B cells Focal Adhesion Kinase (FAK), and find that the numbers of progenitor pro-B, pre-B and immature B cells are reduced by 30–40% in B cell specific FAK knockout mice. When cultured in methylcellulose with IL-7 ± CXCL12, *Fak* deleted pro-B cells yield significantly fewer cells and colonies. Utilizing in situ quantitative imaging cytometry, we establish that in longitudinal femoral bone marrow sections, pro-B cells are preferentially localized in close proximity to the endosteum of the metaphyses and the diaphysis. *Fak* deletion disrupts the non-random distribution of pro-B cells and induces the mobilization of pro-B cells to the periphery *in vivo*. These effects of *Fak* deletion on pro-B cell mobilization and localization in bone marrow are amplified under inflammatory stress, i.e. following immunization with nitrophenol-conjugated chicken γ-globulin in alum (NP-CGG-alum). Collectively, these studies suggest the importance of FAK in regulating pro-B cell homeostasis and maintenance of their spatial distribution in bone marrow niches.

INTRODUCTION

The generation of B lineage cells in the bone marrow (BM) is a dynamic process whereby multi-potent hematopoietic stem cells differentiate into lineage restricted progenitors, which then progress through a series of developmental stages culminating into mature B cells (1). Progenitor B cells have been identified near bone-lining osteoblasts and/or non-hematopoietic stromal cells in BM (2–4). Progenitor B cell growth and maturation are proposed to depend on cues from distinct microenvironments, i.e. niches. Earlier studies, limited to transverse sections of the femoral BM, have proposed that progenitor B cells after sub-lethal irradiation reside close to the endosteal surface of the diaphysis, whereas more mature B cells localized centrally, near the central sinus (5, 6). In addition, the importance of osteoblastic lineage cells in progenitor B cell development has been shown in experimental

Address correspondence and reprint request to Dr. Leslie E. Silberstein, Joint Program in Transfusion Medicine and the Center for Human Cell Therapy Boston, Children's Hospital Boston, 300 Longwood Avenue, Enders 807, Boston, MA 02115, USA. leslie.silberstein@childrens.harvard.edu. Phone: 617-919-2588; Fax: 617-730-0765.
Current address for B. H.: Dept. of Chemical and Biomolecular Engineering Institute for Genomic Biology, University of Illinois at Urbana-Champaign, IL 61801 USA

The online version of this article contains supplemental material.

mouse models (4, 7). More recent data point to the possibility of differentiation-stage specific niches in B cell development (2, 5, 8).

Signals in BM microenvironments might emanate from cell-cell, e.g. VLA-4/VCAM-1, cell-extracellular matrix, e.g. CD44/hyaluronate interactions as well as cellular responses to cytokines, e.g. IL-7, stem cell factor (SCF), FLT3 ligand and chemokines, e.g. CXCL12 (9, 10). Both CXCL12 and its corresponding receptor CXCR4 are essential for progenitor B lymphocyte development (9, 10). CXCL12 is expressed throughout the BM, either in soluble form or immobilized to reticular, endothelial, osteoblast cell types as well as to components of the extracellular matrix (8, 11–14).

Previously, we showed that the CXCL12-induced FAK activation regulates VLA4-mediated cell adhesion to VCAM-1 (CXCL12/CXCR4-FAK-VLA4 pathway) in normal and leukemic progenitor B cells *in vitro*, suggesting that this pathway might modulate progenitor B cell localization in BM niches *in vivo* (15, 16). Furthermore, these studies implicated $G_i\alpha$, Src and Rap1 as intermediary factors (17, 18). FAK, a cytoplasmic tyrosine kinase, has been shown to play an important regulatory function in cell adhesion, motility, growth and survival in response to environmental cues based on initial studies primarily in fibroblasts (19, 20) and subsequently in hematopoietic cells using lineage specific knock out mouse models (21–23). In the current study, we investigated the FAK function in the pro-B cells using B cell-specific *Fak* knockout mice, because of its role as an integrator of external cell signaling downstream of immunoglobulin, growth factor/chemokines and integrin receptors (15, 24, 25). Our findings suggest the importance of FAK in regulating pro-B cell growth and their distinct distribution in the bone marrow microenvironments.

MATERIALS AND METHODS

Experimental animals

Floxed *Fak* mice ($Fak^{fl/fl}$) (26) were crossed to *Cd19-Cre* mice (Jackson Laboratory) to generate *Cd19-Cre*$^{+}$ $Fak^{fl/fl}$ mice. *Cd19-Cre Fak* knock out (KO) mice with the enhanced GFP reporter gene (EGFP^{+} *Cd19-Cre Fak* KO) were produced by crossing *Cd19-Cre*$^{+/-}$ $Fak^{fl/fl}$ mice with Rosa26-EGFP$^{+/-}$ mice provided by Dr. Stuart Orkin (Children's Hospital Boston). The compound mice were backcrossed to C57BL/6 mice (Taconic Farm) for more than 6 generations. Age- and sex-matched CD19-*Cre*$^{+/-}$ $Fak^{wt/wt}$ mice or littermate CD19-*Cre*$^{-/-}$ $Fak^{fl/fl}$ mice, which we found to be phenotypically equivalent, at 8 – 12 weeks of age were used as wild type (WT) controls. The *mb-1-Cre*$^{+/-}$ $Fak^{fl/fl}$ Rosa26-EGFP^{+} mice were generated by crossing $Fak^{fl/fl}$ Rosa26-EGFP$^{+/-}$ with *mb-1-Cre*$^{+/-}$ mice, a generous gift from Dr. Michael Reth (Max-Planck Institute for Immunobiology, Freiburg, Germany). The mb-1-*Cre*$^{+}$ $Fak^{fl/fl}$ mice have higher excision efficiency at the pro-B cell stage and thus yield significantly higher numbers of *Fak* deleted pro-B cells than CD19-*Cre*$^{+}$ $Fak^{fl/fl}$ mice (Fig. S1G and S1H). Animal experiments were performed in accordance with the animal protocols which were approved by the Children's Hospital Boston Animal Care and Use Committee and the Harvard Medical School Standing Committee on Animals.

PCR genotyping

Wild type, floxed, and deleted *Fak* genes were assessed by PCR with primer 1, 2 and 3 as shown in Figure S1A. Primer P1: 5′-GACCTTCAACTTCTCAT TTCTCC-3′; primer P2: 5′-GAATGCTACAGGAACCAAATAAC-3′; primer P3: 5′-GAGAATCCAGCTTTGGCTGTTG-3′. The amplified PCR products consisted of a WT (1.4 kb by P1 and P2 primers; 290 bp by P2 and P3 primers), *Fak-flox* (1.6 kb by P1 and P2 primers; 400 bp by P2 and P3 primers), and *Cre*-mediated recombined fragment (327 bp by P1 and P2 primers) (26). *Cre* genotyping was performed using the PCR primers (forward 5'-

CAAAACAGGTAGTATTCGG, reverse 5'-CGTATAGCCGAAATTGCCAG) as previously described (27). *Egfp* genotyping was performed using the PCR primers (forward 5'-GACCACATGAAGCAGCACG-3', reverse 5'- CCGATGGGGGTGTTCTGC-3') with the conditions, 33 cycles of 93°C for 30 sec, 58°C for 30 sec, and 72°C for 1 min, resulting in a 340-bp product. For *mb1-Cre* genotyping, hCre PCR was used as previously described with the primers hCre dir (5'-CCCTGTGGATGCCACCTC-3') and hCre rev (5'-GTCCTGGCATCTGTCAGAG-3'), resulting in a 450-bp product (28). In contrast to *Cd19-Cre* gene expression, *mb-1-Cre* gene expression starts earlier in B cell development leading to almost complete deletion of floxed genes in BM progenitor B cells (28).

Flow cytometry analysis

Single cell BM suspensions were prepared by crushing and gently grinding the femurs and tibias using a mortar and a pestle in washing buffer (D-PBS, Ca^{2+}-free, Mg^{2+}-free, 2% FBS) followed by hemolysis with ammonium chloride-potassium (ACK) buffer (Gibco BRL). After blocking Fc receptors with anti-CD16/CD32 (2.4G2) antibody, cells were stained with specific antibodies. To sort progenitor B cells, fresh BM cells from iliac bones, femurs, and tibias, were stained with various fluorescent dye- labeled B-lineage specific antibodies (i.e. CD19, B220, CD43, IgM, and IgD). Flow cytometric analysis was carried out on a FACSCanto II (Becton Dickinson), and cell sorting on a FACSAria (Becton Dickinson). The following antibodies were purchased from Becton Dickinson, eBioscience, and/or BioLegend: FITC-, PE-, allophycocyanin-, PE-Cy7-, PerCP-, or allophycocyanin-Cy7-labeled anti- B220 (RA3- 6B2), anti-CD93 (AA4.1), anti-CD43 (S7), anti-CD24/HSA (30F1), anti-BP-1 (6C3), anti-CD117/c-Kit (2B8), anti-CD19 (6D5), anti-CD11b/Mac-1(M1/70), anti-GR1 (Gr-1), anti-IgM (II/41), anti-IgD (11–26), anti-CD21 (7G6), anti-CD23 (33B4).

Colony-forming cell (CFC) assay

In vitro CFC culture assay of pro-B cells was performed using CFC pre-B media (M3630, Stem Cell Tech.) according to the manufacturer's instructions. $B220^{lo}$ IgM^{-} $CD43^{+}$ $EGFP^{+}$ pro-B cells (Fr. B/C/C') were sorted from fresh BM cells and plated in methylcellulose-based IL-7 containing CFC pre-B media (2×10^{3} per plate) in the presence or absence of CXCL12 (500 ng/ml). Colonies containing more than 50 cells were enumerated using an inverted microscope between 3 – 7 days in culture. The cells were harvested from colonies for cell counting and phenotype analysis with different fluorescent dye- labeled CD19, IgM, CD43, and c-Kit antibodies.

Annexin V apoptosis analysis

$B220^{lo}$ IgM^{-} $CD43^{+}$ $EGFP^{+}$ sorted BM cells (2×10^{3} per plate) were plated in IL-7 containing CFC pre-B media (Stem Cell Tech) in the presence or absence of CXCL12 (500 ng/ml). Cells from the CFC colonies were recovered and stained with allophycocyanin-labeled anti-IgM and allophycocyanin-Cy7 labeled anti-CD19 rat antibodies, followed by FITC labeled Annexin V and 7-AAD in Annexin V binding buffer (BD Biosciences). Apoptotic (Annexin V^{+} 7-AAD^{-}) and dead (Annexin V^{+} 7-AAD^{+}) cells were analyzed by a FACSCanto II flow cytometer among the gated $CD19^{+}$ IgM^{-} cell population

Immunofluorescence staining of cryopreserved sections of femurs

Whole mouse femurs were fixed in phosphate-buffered L-lysine with 1% paraformaldehyde/periodate (PLP) more than 4h at 4 °C, followed by washing in 0.1M phosphate buffer pH 7.5, and cryoprotected for 48h in 30% sucrose / 0.1M phosphate buffer. The fixed bones were embedded in OCT compound (optimal cutting temperature compound; a water soluble glycol-resin compound; Sakura Finetek), snap frozen in 2-methylbutane /dry ice mix, and

stored at −80°C. Fresh cryopreserved, non-decalcified femurs were sectioned longitudinally at 4–5 μm thickness to facilitate in situ laser scanning cytometry analysis of a single cell-thick layer using the CryoJane tape-transfer system (Instrumedics) in a cryostat (LEICA CM1800). All sections were prepared from the middle of the femur to include the central sinus. Thawed frozen sections were thoroughly air dried and rehydrated in D-PBS. The sections were blocked in blocking medium (10% normal donkey serum / 0.025% Tween-20 in Ca^{2+}-free, Mg^{2+}-free D-PBS) for 1h followed by streptavidin/biotin blocking solution (Vector Laboratories). The sections were stained with rat anti-CD43 antibody (S7, BD Biosciences) or rat anti-IgD antibody (11-26c, BioLegend), followed by Dylight 488-labeled donkey anti-rat IgG (Jackson ImmunoResearch). After blocking with normal rat serum, the sections were stained with biotin-labeled rat anti-B220 (RA3- 6B2, eBioscience), followed by Dylight 549- labeled streptavidin (Jackson ImmunoResearch). For niche staining, sections were stained with goat anti-osteopontin antibody (R&D Systems) for osteoblasts, rabbit anti-laminin (Chemicon) for vasculature, or goat anti-CD105 (endoglin) antibody (R&D Systems) for sinusoids followed by Dylight 649-labeled donkey antiserum antibody (Jackson ImmunoResearch). For Rosa26-GFP^+ *Fak* WT or KO mice, we used chicken anti-GFP antibody (Invitrogen), rat anti-CD43 antibody (S7, BD Biosciences), and goat anti-osteopontin antibody (R&D Systems), followed by staining with Dylight dye-labeled donkey antiserum antibodies (Jackson ImmunoResearch). Pro-B cells were identified by GFP^+ $CD43^+$ cells. Dilutions of primary and secondary antibodies were optimized for laser scanning cytometry and confocal microscopy imaging. Isotype control slides were stained with Dylight 549-, Dylight 649-, or Dylight 488-labeled secondary antibodies after isotype control primary antibody staining. All slides were then labeled with 1 μM DAPI for 3 min (Invitrogen) and coverslips were placed using slow-fade mounting media (Molecular Probes).

In situ solid phase laser scanning cytometry (LSC) analysis

For all LSC analyses, the iCys® Research Imaging Cytometer (CompuCyte Corp.) with four excitation lasers (405, 488, 561, and 633 nm), four emission filters (425–455, 500–550, 575–625, 650nm long pass), and four photomultiplier tubes (PMT). For each fluorescent marker, images are built pixel by pixel from the quantitative PMT measurements of laser-spot-excited fluorescence signals (29). The quantitative imaging cytometry control software generated a single ‘Region’ image of the entire BM cavity from a sequence of high-magnification (40× / NA 0.95 dry objective) ‘Field’ immunofluorescence images (250 μm × 190 μm per field image) which were subjected to automated analysis of contour-based cellular events, their fluorescence levels, and their location within the BM section. Bone lining was identified by autofluorescence of the collagen in bone. Individual cellular events are defined by threshold contouring of DAPI stained nuclei. In longitudinal BM sections, each femoral scan produces average of 100,000 cellular events. The total fluorescence intensity from individual cellular events is measured in each channel within the integration contour. The integration contour is set as 2 pixels out from the threshold contour, a value which is based on the size of the cell, to allow definition of the edge of the cell (pixel size is 0.25 μm × 0.25 μm). Isotype antibodies were used as negative controls for gating purposes. The total number and morphological distribution of each distinct cellular subpopulation within the entire femoral BM cavity or at specific anatomical locations within the cavity can then be determined using post-scan automated image analysis software (iCys® cytometric analysis software, CompuCyte Corp.). To assess statistical significance, a minimum of three distinct frozen sections were analyzed from each femur from a minimum of 4 *Fak* KO and 4 WT control animals. LSC analysis in cryopreserved splenic tissue was performed to validate the quantitative imaging cytometry technology because of its well characterized B cell compartments. The percentage of $B220^+$ B cells determined via flow cytometry (50%) and LSC (42 ± 6.3%, mean ± SEM) in splenic mononuclear cells was comparable (Fig. S3A), if

taking under consideration that the laser scanning cytometer also quantifies adherent splenic cells, e.g. fibroblasts, endothelial cells. Imaging cytometry further allowed for global characterization of the follicular organization of $B220^+$ B-cells in spleen (Fig. S3A). H&E staining of non-decalcified, cryopreserved, 5μm-thick, longitudinal femur sections demonstrates the integrity of BM tissue architecture (Fig. S3B).

Homing analysis

$B220^+$ $CD43^+$ $EGFP^+$ pro-B cells were sorted from mb-1-Cre^+ $Fak^{fl/fl}$ ROSA26-$EGFP^+$ KO and mb1-Cre^+ $Fak^{wt/wt}$ ROSA26-$EGFP^+$ WT mice by FACSAria (Becton Dickinson). Sorted $B220^+$ $CD43^+$ $EGFP^+$ pro-B cells from *Fak* KO or WT were differentially labeled with chloromethyl derivatives of fluorescein diacetate (CMFDA) dye and chloromethyl derivatives of aminocoumarin (CMAC) dye. 5-(and-6)-(((4-chloromethyl)benzoyl)amino) tetramethylrhodamine (CMTMR)-labeled WT splenic B cells were co-injected as reference cells. 1×10^6 each labeled cells were mixed, and intravenously transferred to wild type C57BL/6 recipient mice. Some input cells were saved to assess the concentration of transferred *Fak* KO cells and WT cells. After 2 hrs, *in vivo* selective labeling of intravascular B cells was performed by injecting the recipient mice with 1 μg of PE-Cy7 labeled anti-B220 antibodies for 2 min as described by J.P. Pereira et al.(30). The recipient mice were sacrificed, followed by harvesting cardiac blood, spleen, and BM. The frequency of total cells that homed to BM as well as the fraction present intravascularly was determined by FACS. For the BM, the number of homed cells was calculated by multiplying the number of cells harvested from a hind leg by 14.3, assuming that 1 limb contains ~7% of all BM cells (31). Intravascular B cells were determined by *in vivo* PE-Cy7 labeling.

Statistical analysis

Statistical analysis was performed on all numerical data as indicated each figure using GraphPad Prism software (GraphPad, San Diego, CA).

RESULTS

Fak deletion causes a selective decrease in BM progenitor B and immature B cells

Fak was conditionally deleted in B cells by breeding $Fak^{fl/fl}$ mice with CD19-$Cre^{+/-}$ mice to generate CD19-$Cre^{+/-}$ $Fak^{fl/fl}$ mice, i.e. CD19-Cre *Fak* knockout (from now on termed *Fak* KO). PCR and immunoblotting analysis of sorted BM or spleen cells showed that *Fak* deletion was evident beginning at the pro-B cell stage and was associated with absence of FAK protein (Fig. S1A–E). Progenitor B cell populations, e.g. $CD19^+$ $B220^{lo}$ $CD43^+$ IgM^-, $CD19^+$ $B220^{lo}$ $CD43^-$ IgM^-, and $CD19^+$ $B220^{lo}$ $AA4.1^+$ IgM^+ immature B cells were reduced by 30–40% compared to wild type (WT) control mice (Fig.1A). Similarly, newly emigrated immature B cells from BM, e.g. T1 B cells in spleen, also were reduced by 30–40% (Fig. S2B and S2C), while the follicular and marginal zone B cell compartments were unaffected (Fig. S2A). The total number of BM $B220^+$ B cells in CD19-Cre *Fak* KO was reduced by 30% compared to WT control mice. In contrast, the numbers of re-circulating mature B cells in BM and mature B cells in peripheral blood and spleen ($CD19^+$ $AA4.1^-$ $IgM^{+/lo}$ IgD^+ cells), were similar in CD19-Cre *Fak* KO and WT control mice WT (Fig.1A and B), even though these mature B cell populations exhibited efficient *Fak* deletion (Fig.S1C and S1D). Subsequently, the selective decrease of progenitor B cells and immature B cells in the BM was confirmed in mb1-Cre^+ $Fak^{fl/fl}$ KO mice (Fig. 1C). *Fak* deletion did not cause a change in CXCR4 and VLA-4 surface expression on B cells from BM and spleen (data not shown). Moreover, expression of the FAK- related tyrosine kinase Pyk-2 was not increased in *Fak* deleted progenitor and mature B cells (Fig. S1E); similarly Pyk-2 compensation was not observed in *Fak* deleted megakaryocytes, neuronal and embryonic endothelial cells (26, 32).

Fak deletion affects progenitor B cell growth

Given the selective decrease in progenitor B cell populations in BM of *Fak* KO mice (Fig. 1A), we theorized that *Fak* deletion might influence pro-B cell growth in response to progenitor B cell cyto/chemokines. To explore this possibility, CD19-$Cre^{+/-}$ $Fak^{fl/fl}$ Rosa26-$EGFP^{+/-}$ mice were generated in which EGFP expression correlates with efficient *Fak* gene deletion (Fig.S1F). Colony forming cell assays with IL-7 were performed in the presence and absence of CXCL12 to examine the effect of CXCL12 signaling on pro-B cell growth. The number of colony forming cell (CFC) colonies and total cell number from *Fak* deleted $B220^{lo}$ IgM^- $CD43^+$ $EGFP^+$ pro-B cells cultured in IL-7 ± CXCL12 were 40–50% lower compared to the number of colonies and cells from WT $B220^{lo}$ IgM^- $CD43^+$ $EGFP^+$ pro-B cells (Fig. 2A). Of interest, $B220^{lo}$ IgM^- $CD43^-$ pre-B cells did not generate colonies in IL-7 ± CXCL12 methylcellulose (data not shown). CXCL12 acted synergistically with IL-7 to promote colony formation and cell growth in WT mice and *Fak* KO mice (Fig. 2A). Flow cytometry performed on CFC cells from both WT and *Fak* KO mice retrieved on day 7 of culture showed that >80% were IgM^- progenitor B cells, of which 20% and 14% are c-Kit^+ pro-B cells, respectively (Fig. 2B). The colony re-plating assay is an *in vitro* surrogate assay in which re-plating capacity of colony forming cells reflects the limited self-renewal capacity of hematopoietic precursor cells, including pro-B cells (33, 34). As shown in Figure 2C, the number of secondary colonies derived from *Fak* deleted pro-B cells was significantly reduced indicating that *Fak* deletion reduces the re-plating activity of pro-B cells. Finally, further investigation of the in vitro cultures showed that *Fak* deletion also promoted cell apoptosis: the fraction of apoptotic cells was significantly higher (ranging from 50–70%) in *Fak*-deleted progenitor B cells compared to WT progenitor B cells beginning on day 4 and maximizing on day 7 of CFC culture (Fig. 2D).

Non-random, gradient distribution of pro-B cells in longitudinal sections of femoral BM

Although highly desirable, a comprehensive analysis of the global spatial distribution of phenotypically defined B cell populations in the context of entire BM cavities has not been carried out. This is mostly due to the technical difficulties associated with imaging of long bones and the need for cell-surface marker combinations used to track B cell populations at a single cell level. To this end, we employed Laser Scanning Cytometry (LSC), which provided a detailed quantitative map of the spatial distribution of B cell subsets in whole-longitudinal femoral BM sections (Fig. S4A–D). The fluorescence levels associated with each cellular event are measured and plotted while retaining the localization of the cellular event within the entire longitudinal BM section (Fig. S4D and 3A). This approach allows for the generation of tissue maps (Fig. 3B) and the objective quantification of discrete B cell subsets within different regions, e.g. microenvironments. Distribution data are shown for pro-B cell and mature B cell stage populations, e.g. $B220^+$ $CD43^+$ and $B220^+$ IgD^+ B cells, respectively (Fig. 3A–F). While B cells of all stages were found throughout the BM cavity, the distribution of pro-B cells differed from that of mature B cells. $B220^+$ $CD43^+$ pro-B cells were localized preferentially in the metaphyses, whereas mature B cells were preferentially in the diaphysis (Fig. 3C). Moreover, within the diaphysis pro-B cells localized predominantly in the endosteal region (< 100 μm from the endosteum), whereas mature B cells tended to localize outside the endosteal region (Fig. 3D). In addition, the distance to endosteal surface was measured for individual pro-B cells and mature B cells in longitudinal BM sections. The collective data illustrate a distinctive non-random gradient distribution of pro-B cells with a high predilection for the endosteum (Fig. 3E and 3F).

FAK regulates the distribution of pro-B cells in femoral BM microenvironments

Because FAK phosphorylation can be triggered via chemokine, antigen and integrin receptors on B cells (15, 24, 25), we hypothesized that FAK also might regulate the distribution of $B220^+$ $CD43^+$ pro-B cells in the BM cavity. By quantitative imaging analyses

of longitudinal sections of femurs, we found that in comparison to WT mice, the lodgment of pro-B cells is significantly altered in *Fak* KO mice, resulting in an even distribution in the metaphyses and diaphyses (Fig. 4A). Moreover, their striking close proximity to the endosteum is no longer evident as the accumulated fraction of pro-B cells in the endosteal region is reduced by 50% (Fig. 4B). We explored this observation more specifically and determined that *Fak* deletion impairs the close proximity of pro-B cells to osteopontin^{+} bone lining osteoblasts in the metaphyses (Fig. 4C). We also confirmed the impairment of pro-B cell distribution in the BM of mb1-Cre^{+} *Fak*$^{fl/fl}$ KO mice (Fig. 4D). Thus, we conclude that FAK influences the localization of pro-B cells in BM microenvironments.

Fak deletion leads to mobilization of pro-B cells to the periphery

We considered that *Fak* deletion might also cause a defect in pro-B cell retention in BM and thus enhance the egress of pro-B cells to the periphery. An increase in the number of CD19^{+} B220^{+} IgM^{-} progenitor B cells could not be discerned with confidence by flow cytometry in peripheral blood or spleen of *Fak* KO (not shown). Thus, the methyl cellulose-based colony forming cell (CFC) assay was applied as this method has been used to quantitate low numbers of mobilized hematopoietic progenitor cells in peripheral blood (35). By the CFC assay, significantly increased numbers of pro-B cells were detected in peripheral blood of *Fak* KO compared to control WT mice (Fig. 5A). The 7-day colony forming cells were then analyzed by flow cytometry and shown to be mainly CD19^{+} B220^{+} IgM^{-} progenitor B cells of which 22% were c-Kit^{+} pro-B cells (Fig. 5B); we assessed for c-Kit surface expression rather than CD43 expression because the latter marker remains high during differentiation of pro-B cells grown in IL-7 containing culture conditions (36), We confirmed that these progenitor B cells were *Fak* deleted as determined by PCR (Fig. 5C).

We next reasoned that FAK function might be further manifested under stress conditions, such as immunization with the inflammatory antigen nitrophenol-conjugated chicken γ-globulin in alum (NP-CGG-alum), which induces significant progenitor B cell mobilization to the periphery(37). To this end, the presence of B220^{lo} CD19^{+} IgM^{-} IgD^{-} CD93^{+} progenitor B cells, of which 42% are c-Kit^{+} pro-B cells, was analyzed in the spleen and peripheral blood after immunization (Fig. 5D). FACS analyses showed that the percentages of B220^{lo} CD19^{+} IgM^{-} CD93^{+} progenitor B cells gradually increased from day 4 up to day 14 in the spleen and blood. However, the percentages of progenitor B cells increased substantially (>2.5–3 times) more in *Fak* KO mice (Fig. 5E and 5F). Immunization of alum alone produced similar results as immunization with NP-CGG-alum (data not shown), indicating that the egress of pro-B cells is induced by inflammatory immunization, and thus is not antigen dependent. Concomitantly by LSC analysis of femoral sections, immunization with NP-CGG-Alum led to a reduction in the percentage of B220^{+} CD43^{+} pro-B cells in the endosteal zones (< 5 microns of osteopontin+ bone lining osteoblasts), which also was significantly more noticeable in *Fak* KO mice (Fig. 5G and 5H). Taken together, these data suggest that FAK plays an important role in the retention of progenitor B cells in BM.

Pro-B cell homing to the BM cavity is regulated by FAK

Since homing and engraftment of hematopoietic stem and progenitor cells are dependent on the coordinated function of cyto/chemokines, e.g. CXCL12 (38), and adhesion molecules, e.g. VCAM-1, (39), we hypothesized that FAK also might be important in the engraftment of intravenously infused pro-B cells (40), Homing experiments showed that the number of homed pro-B cells was significantly reduced for *Fak* deleted compared to WT pro-B cells (Fig. 6A). Noteworthy, was the striking reduction in number of homed *Fak* deleted pro-B cells, which had lodged in the extravascular compartment of BM. In contrast, the number of homed pro-B cells localized intravascularly was equivalent for *Fak* deleted and WT pro-B cells (Fig. 6A and 6B).

DISCUSSION

Niches defined within disparate anatomical regions of the bone marrow cavity are thought to provide distinct cues for the growth, differentiation and survival of hematopoietic stem and progenitor cells. Prior studies (15, 17, 18) on the role of the CXCR4-FAK-VLA-4 pathway in progenitor B cells led us to examine FAK function *in vivo* and to test the hypothesis that FAK, by coordinating signaling via chemo/cytokine and adhesion receptors, might play an important role in progenitor B cell lodgment in bone marrow. *Cre*-mediated *Fak* deletion results in a decrease in pro-B, pre-B and immature B cell populations in the BM. In contrast, the mature B cell compartments in the BM and spleen are unaffected. This likely occurs because in *Fak* KO mice, adequate numbers of immature B cells are generated, which subsequently fill the mature B cell compartment in peripheral lymphoid organs similar to what has been observed in normal B cell development and other gene targeted mouse models (4, 41). To further explore the underlying reasons accounting for the decrease in progenitor B cells in the bone marrow of *Fak* KO mice, we first considered that FAK function might play an important role in pro-B cell growth. To explore this possibility, the cytokine supplemented CFC methylcellulose assay was used since it is a well established assay for growth studies on hematopoietic stem/progenitor cells (42, 43). While IL-7 is the standard cytokine used for the CFU-B assay (44), we explored the addition of CXCL12 since it is considered essential for early stages of B cell development (10, 45). CXCL12 acted synergistically with IL-7 to promote colony formation and cell growth of WT and *Fak* deleted pro-B cells (Fig. 2A). The exact molecular mechanism for this observation is unclear but is likely related to the multiple cytoplasmic and nuclear FAK pathways, which promote cell growth and survival. We find that *Fak* deleted cells generate a significantly lower number of progenitor B cells and colonies. Moreover, *Fak* deleted cells have impaired colony re-plating potential, a feature, which has been ascribed to the distinct *ex vivo* clonability of pro-B cells (46). *Fak* deleted pro-B cells undergo increased apoptosis in culture, which contributes to their impaired growth. One mechanism for the pro-survival function of FAK, is its regulation of p53 (47), which mediates activation of effector caspases during apoptosis (48). In this regard, evidence for caspase-3 mediated apoptosis in *Fak* deleted pro-B cell lines was previously reported (49).

Although the association of pro-B cells with specific BM niche cells, such as $CXCL12^+$ abundant reticulocytes or $IL\text{-}7^+$ stromal cells, has been reported (8), the global distribution of pro-B cells in the entire femur cavity remains unknown to date. Using quantitative imaging cytometry technique LSC we report a distinctive non-random gradient distribution of pro-B cells with a high predilection for the endosteum (Fig. 3E and 3F). The observed gradient in pro-B cell distribution may be the consequence of several processes. It is conceivable that even the most primitive committed lymphoid progenitor cells already have a gradient distribution. Alternatively, differentiating progenitor B cells migrate within the BM compartment and their ultimate location is influenced by differences in composition and/or availability of B cell specific niches in the endosteal region versus the central medullary region which contains the central sinus.

The disruption of the non-random, gradient distribution of pro-B cells in the BM (Fig. 4) by *Fak* deletion suggests that the distribution of pro-B cells is regulated by niche-induced FAK signaling pathway, supporting the previously proposed function of FAK in the CXCL12-induced cell adhesion to VCAM-1 *in vitro* studies (15, 17, 18). Further studies are needed to understand the physiological significance of the distinctive non-random gradient distribution of pro-B cells in the BM. Interestingly, *Fak* deletion also leads to the egress of pro-B cells into the peripheral circulation. This mobilization was further augmented by immunization with the inflammatory immunogen NP-CGG-alum, which causes a reduction of CXCL12 expression in the bone marrow under inflammatory conditions coincident with egress of

progenitor B cells and impaired B lymphopoiesis (37). It is reasonable to speculate that in *Fak* deleted pro- B cells the CXCR4-FAK-VLA-4 pathway is impaired since inhibition of CXCR4/CXCL12 and/or VLA-4/VCAM-1 axes leads to the mobilization of hematopoietic stem and progenitor cells (50–53). Together, the data suggest that disruption of the interaction between pro-B cells and niche cells contributes to impaired B lymphopoiesis and possibly in leukemia development since FAK also plays an important function in malignancy, including acute myelogenous leukemia (54–56). Moreover, FAK silencing inhibits leukemogenesis of BCR/ABL-transformed pro-B (BaF3) cells (49). Thus, further definition of the complexity of niche components, e.g. vascular and diverse stromal cell types, and the signaling pathways they trigger may provide further insight into B cell development and potentially offer therapeutic targets of leukemia.

Supplementary Material

Refer to Web version on PubMed Central for supplementary material.

Acknowledgments

We thank Drs. C. Walkley and S. Orkin (Children's Hospital Boston) for Rosa26-EGFP$^{+/-}$ mice; Dr. Michael Reth (Max-Planck Institute for Immunobiology, Freiburg, Germany) and Dr. Klaus Rajewsky (Harvard Medical School, Boston MA) for Mb-1-Cre mice; N. Calderone (Brigham & Women's Hospital) for cryosectioning of femoral bones; CompuCyte (Westwood, MA) for LSC technical help.

This work was supported by the National Institutes of Health (5T32 HL066987, 1R21 HL094923, 1RO1 HL093139, U24 HL074355).

Abbreviations used in this article

7-AAD	7-Aminoactinomycin D
BM	bone marrow
CFC	colony forming cell
FAK	Focal Adhesion Kinase
KO	knockout
LSC	Laser Scanning Cytometry
NP-CGG	Nitrophenol-conjugated chicken γ-globulin
PB	peripheral blood
WT	wild type

REFERENCES

1. Hardy RR, Hayakawa K. B cell development pathways. Annu Rev Immunol. 2001; 19:595–621. [PubMed: 11244048]
2. Nagasawa T. Microenvironmental niches in the bone marrow required for B-cell development. Nat Rev Immunol. 2006; 6:107–116. [PubMed: 16491135]
3. Visnjic D, Kalajzic Z, Rowe DW, Katavic V, LorenzoH J, Aguila HL. Hematopoiesis is severely altered in mice with an induced osteoblast deficiency. Blood. 2004; 103:3258–3264. [PubMed: 14726388]
4. Wu JY, Purton LE, Rodda SJ, Chen M, Weinstein LS, McMahon AP, Scadden DT, Kronenberg HM. Osteoblastic regulation of B lymphopoiesis is mediated by Gs{alpha}-dependent signaling pathways. Proc Natl Acad Sci U S A. 2008; 105:16976–16981. [PubMed: 18957542]

5. Osmond DG, Kim N, Manoukian R, Phillips RA, Rico-Vargas SA, Jacobsen K. Dynamics and localization of early B-lymphocyte precursor cells (pro-B cells) in the bone marrow of scid mice. Blood. 1992; 79:1695–1703. [PubMed: 1373084]
6. Jacobsen K, Tepper J, Osmond DG. Early B-lymphocyte precursor cells in mouse bone marrow: subosteal localization of B220+ cells during postirradiation regeneration. Exp Hematol. 1990; 18:304–310. [PubMed: 2323366]
7. Zhu J, Garrett R, Jung Y, Zhang Y, Kim N, Wang J, Joe GJ, Hexner E, Choi Y, Taichman RS, Emerson SG. Osteoblasts support B-lymphocyte commitment and differentiation from hematopoietic stem cells. Blood. 2007; 109:3706–3712. [PubMed: 17227831]
8. Tokoyoda K, Egawa T, Sugiyama T, Choi BI, Nagasawa T. Cellular niches controlling B lymphocyte behavior within bone marrow during development. Immunity. 2004; 20:707–718. [PubMed: 15189736]
9. Ma Q, Jones D, Borghesani PR, Segal RA, Nagasawa T, Kishimoto T, Bronson RT, Springer TA. Impaired B-lymphopoiesis, myelopoiesis, and derailed cerebellar neuron migration in CXCR4- and SDF-1-deficient mice. Proc Natl Acad Sci U S A. 1998; 95:9448–9453. [PubMed: 9689100]
10. Nagasawa T, Hirota S, Tachibana K, Takakura N, Nishikawa S, Kitamura Y, Yoshida N, Kikutani H, Kishimoto T. Defects of B-cell lymphopoiesis and bone-marrow myelopoiesis in mice lacking the CXC chemokine PBSF/SDF-1. Nature. 1996; 382:635–638. [PubMed: 8757135]
11. Dar A, Goichberg P, Shinder V, Kalinkovich A, Kollet O, Netzer N, Margalit R, Zsak M, Nagler A, Hardan I, Resnick I, Rot A, Lapidot T. Chemokine receptor CXCR4-dependent internalization and resecretion of functional chemokine SDF-1 by bone marrow endothelial and stromal cells. Nat Immunol. 2005; 6:1038–1046. [PubMed: 16170318]
12. Peled A, Grabovsky V, Habler L, Sandbank J, Arenzana-Seisdedos F, Petit I, Ben-Hur H, Lapidot T, Alon R. The chemokine SDF-1 stimulates integrin-mediated arrest of CD34(+) cells on vascular endothelium under shear flow. J Clin Invest. 1999; 104:1199–1211. [PubMed: 10545519]
13. Jung Y, Wang J, Schneider A, Sun YX, Koh-Paige AJ, Osman NI, McCauley LK, Taichman RS. Regulation of SDF-1 (CXCL12) production by osteoblasts; a possible mechanism for stem cell homing. Bone. 2006; 38:497–508. [PubMed: 16337237]
14. Amara A, Lorthioir O, Valenzuela A, Magerus A, Thelen M, Montes M, Virelizier JL, Delepierre M, Baleux F, Lortat-Jacob H, Arenzana-Seisdedos F. Stromal cell-derived factor-1alpha associates with heparan sulfates through the first beta-strand of the chemokine. J Biol Chem. 1999; 274:23916–23925. [PubMed: 10446158]
15. Glodek AM, Honczarenko M, Le Y, Campbell JJ, Silberstein LE. Sustained activation of cell adhesion is a differentially regulated process in B lymphopoiesis. J Exp Med. 2003; 197:461–473. [PubMed: 12591904]
16. Le Y, Zhu BM, Harley B, Park SY, Kobayashi T, Manis JP, Luo HR, Yoshimura A, Hennighausen L, Silberstein LE. SOCS3 protein developmentally regulates the chemokine receptor CXCR4-FAK signaling pathway during B lymphopoiesis. Immunity. 2007; 27:811–823. [PubMed: 18031698]
17. Glodek AM, Le Y, Dykxhoorn DM, Park SY, Mostoslavsky G, Mulligan R, Lieberman J, Beggs HE, Honczarenko M, Silberstein LE. Focal adhesion kinase is required for CXCL12-induced chemotactic and pro-adhesive responses in hematopoietic precursor cells. Leukemia. 2007; 21:1723–1732. [PubMed: 17568820]
18. Le Y, Honczarenko M, Glodek AM, Ho DK, Silberstein LE. CXC chemokine ligand 12-induced focal adhesion kinase activation and segregation into membrane domains is modulated by regulator of G protein signaling 1 in pro-B cells. J Immunol. 2005; 174:2582–2590. [PubMed: 15728464]
19. Parsons JT. Focal adhesion kinase: the first ten years. J Cell Sci. 2003; 116:1409–1416. [PubMed: 12640026]
20. Mitra SK, Hanson DA, Schlaepfer DD. Focal adhesion kinase: in command and control of cell motility. Nat Rev Mol Cell Biol. 2005; 6:56–68. [PubMed: 15688067]
21. Hitchcock IS, Fox NE, Prevost N, Sear K, Shattil SJ, Kaushansky K. Roles of focal adhesion kinase (FAK) in megakaryopoiesis and platelet function: studies using a megakaryocyte lineage specific FAK knockout. Blood. 2008; 111:596–604. [PubMed: 17925492]

22. Kasorn A, Alcaide P, Jia Y, Subramanian KK, Sarraj B, Li Y, Loison F, Hattori H, Silberstein LE, Luscinskas WF, Luo HR. Focal adhesion kinase regulates pathogen-killing capability and life span of neutrophils via mediating both adhesion-dependent and -independent cellular signals. J Immunol. 2009; 183:1032–1043. [PubMed: 19561112]
23. Vemula S, Ramdas B, Hanneman P, Martin J, Beggs HE, Kapur R. Essential role for focal adhesion kinase in regulating stress hematopoiesis. Blood. 2010; 116:4103–4115. [PubMed: 20664055]
24. Manie SN, Astier A, Wang D, Phifer JS, Chen J, Lazarovits AI, Morimoto C, Freedman AS. Stimulation of tyrosine phosphorylation after ligation of beta7 and beta1 integrins on human B cells. Blood. 1996; 87:1855–1861. [PubMed: 8634433]
25. Mlinaric-Rascan I, Yamamoto T. B cell receptor signaling involves physical and functional association of FAK with Lyn and IgM. FEBS Lett. 2001; 498:26–31. [PubMed: 11389892]
26. Beggs HE, Schahin-Reed D, Zang K, Goebbels S, Nave KA, Gorski J, Jones KR, Sretavan D, Reichardt LF. FAK deficiency in cells contributing to the basal lamina results in cortical abnormalities resembling congenital muscular dystrophies. Neuron. 2003; 40:501–514. [PubMed: 14642275]
27. Rickert RC, Roes J, Rajewsky K. B lymphocyte-specific, Cre-mediated mutagenesis in mice. Nucleic Acids Res. 1997; 25:1317–1318. [PubMed: 9092650]
28. Hobeika E, Thiemann S, Storch B, Jumaa H, Nielsen PJ, Pelanda R, Reth M. Testing gene function early in the B cell lineage in mb1-cre mice. Proc Natl Acad Sci U S A. 2006; 103:13789–13794. [PubMed: 16940357]
29. Grierson AM, Mitchell P, Adams CL, Mowat AM, Brewer JM, Harnett MM, Garside P. Direct quantitation of T cell signaling by laser scanning cytometry. J Immunol Methods. 2005; 301:140–153. [PubMed: 15990109]
30. Pereira JP, An J, Xu Y, Huang Y, Cyster JG. Cannabinoid receptor 2 mediates the retention of immature B cells in bone marrow sinusoids. Nat Immunol. 2009; 10:403–411. [PubMed: 19252491]
31. Colvin GA, Lambert JF, Abedi M, Hsieh CC, Carlson JE, Stewart FM, Quesenberry PJ. Murine marrow cellularity and the concept of stem cell competition: geographic and quantitative determinants in stem cell biology. Leukemia. 2004; 18:575–583. [PubMed: 14749701]
32. Shen TL, Park AY, Alcaraz A, Peng X, Jang I, Koni P, Flavell RA, Gu H, Guan JL. Conditional knockout of focal adhesion kinase in endothelial cells reveals its role in angiogenesis and vascular development in late embryogenesis. J Cell Biol. 2005; 169:941–952. [PubMed: 15967814]
33. Hardy RR, Carmack CE, Li YS, Hayakawa K. Distinctive developmental origins and specificities of murine CD5+ B cells. Immunol Rev. 1994; 137:91–118. [PubMed: 7518415]
34. Broxmeyer HE, Mejia JA, Hangoc G, Barese C, Dinauer M, Cooper S. SDF-1/CXCL12 enhances in vitro replating capacity of murine and human multipotential and macrophage progenitor cells. Stem Cells Dev. 2007; 16:589–596. [PubMed: 17784832]
35. Yang FC, Atkinson SJ, Gu Y, Borneo JB, Roberts AW, Zheng Y, Pennington J, Williams DA. Rac and Cdc42 GTPases control hematopoietic stem cell shape, adhesion, migration, and mobilization. Proc Natl Acad Sci U S A. 2001; 98:5614–5618. [PubMed: 11320224]
36. Corfe SA, Gray AP, Paige CJ. Generation and characterization of stromal cell independent IL-7 dependent B cell lines. J Immunol Methods. 2007; 325:9–19. [PubMed: 17599344]
37. Ueda Y, Yang K, Foster SJ, Kondo M, Kelsoe G. Inflammation controls B lymphopoiesis by regulating chemokine CXCL12 expression. J Exp Med. 2004; 199:47–58. [PubMed: 14707114]
38. Lapidot T, Kollet O. The essential roles of the chemokine SDF-1 and its receptor CXCR4 in human stem cell homing and repopulation of transplanted immune-deficient NOD/SCID and NOD/SCID/B2m(null) mice. Leukemia. 2002; 16:1992–2003. [PubMed: 12357350]
39. Frenette PS, Subbarao S, Mazo IB, von Andrian UH, Wagner DD. Endothelial selectins and vascular cell adhesion molecule-1 promote hematopoietic progenitor homing to bone marrow. Proc Natl Acad Sci U S A. 1998; 95:14423–14428. [PubMed: 9826716]
40. Hardy R, Hayakawa K. Generation of Ly-1 B cells from developmentally distinct precursors. Enrichment by stromal-cell culture or cell sorting. Ann N Y Acad Sci. 1992; 651:99–111. [PubMed: 1376094]

41. Allman DM, Ferguson SE, Lentz VM, Cancro MP. Peripheral B cell maturation. II. Heat-stable antigen(hi) splenic B cells are an immature developmental intermediate in the production of long-lived marrow-derived B cells. J Immunol. 1993; 151:4431–4444. [PubMed: 8409411]
42. Bradley TR, Metcalf D. The growth of mouse bone marrow cells in vitro. Aust J Exp Biol Med Sci. 1966; 44:287–299. [PubMed: 4164182]
43. Pierre-Louis O, Clay D, Brunet de la Grange P, Blazsek I, Desterke C, Guerton B, Blondeau C, Malfuson JV, Prat M, Bennaceur-Griscelli A, Lataillade JJ, Le Bousse-Kerdiles MC. Dual SP/ALDH functionalities refine the human hematopoietic Lin-CD34+CD38-stem/progenitor cell compartment. Stem Cells. 2009; 27:2552–2562. [PubMed: 19650038]
44. Kincade PW, Lee G, Scheid MP, Blum MD. Characterization of murine colony-forming B cells. II. Limits to in vitro maturation, Lyb-2 expression, resolution of IgD+ subsets, and further population analysis. J Immunol. 1980; 124:947–953. [PubMed: 6965394]
45. Nagasawa T, Kikutani H, Kishimoto T. Molecular cloning and structure of a pre-B-cell growth-stimulating factor. Proc Natl Acad Sci U S A. 1994; 91:2305–2309. [PubMed: 8134392]
46. Rolink A, Haasner D, Nishikawa S, Melchers F. Changes in frequencies of clonable pre B cells during life in different lymphoid organs of mice. Blood. 1993; 81:2290–2300. [PubMed: 7683215]
47. Lim ST, Chen XL, Lim Y, Hanson DA, Vo TT, Howerton K, Larocque N, Fisher SJ, Schlaepfer DD, Ilic D. Nuclear FAK promotes cell proliferation and survival through FERM-enhanced p53 degradation. Mol Cell. 2008; 29:9–22. [PubMed: 18206965]
48. Yu Y, Little JB. p53 is involved in but not required for ionizing radiation-induced caspase-3 activation and apoptosis in human lymphoblast cell lines. Cancer Res. 1998; 58:4277–4281. [PubMed: 9766652]
49. Le Y, Xu L, Lu J, Fang J, Nardi V, Chai L, Silberstein LE. FAK silencing inhibits leukemogenesis in BCR/ABL-transformed hematopoietic cells. Am J Hematol. 2009; 84:273–278. [PubMed: 19358301]
50. Papayannopoulou T, Craddock C, Nakamoto B, Priestley GV, Wolf NS. The VLA4/VCAM-1 adhesion pathway defines contrasting mechanisms of lodgement of transplanted murine hemopoietic progenitors between bone marrow and spleen. Proc Natl Acad Sci U S A. 1995; 92:9647–9651. [PubMed: 7568190]
51. Papayannopoulou T, Nakamoto B. Peripheralization of hemopoietic progenitors in primates treated with anti-VLA4 integrin. Proc Natl Acad Sci U S A. 1993; 90:9374–9378. [PubMed: 7692447]
52. Ma Q, Jones D, Springer TA. The chemokine receptor CXCR4 is required for the retention of B lineage and granulocytic precursors within the bone marrow microenvironment. Immunity. 1999; 10:463–471. [PubMed: 10229189]
53. Broxmeyer HE, Orschell CM, Clapp DW, Hangoc G, Cooper S, Plett PA, Liles WC, Li X, Graham-Evans B, Campbell TB, Calandra G, Bridger G, Dale DC, Srour EF. Rapid mobilization of murine and human hematopoietic stem and progenitor cells with AMD3100, a CXCR4 antagonist. J Exp Med. 2005; 201:1307–1318. [PubMed: 15837815]
54. Tilghman RW, Parsons JT. Focal adhesion kinase as a regulator of cell tension in the progression of cancer. Semin Cancer Biol. 2008; 18:45–52. [PubMed: 17928235]
55. McLean GW, Carragher NO, Avizienyte E, Evans J, Brunton VG, Frame MC. The role of focal-adhesion kinase in cancer - a new therapeutic opportunity. Nat Rev Cancer. 2005; 5:505–515. [PubMed: 16069815]
56. Recher C, Ysebaert L, Beyne-Rauzy O, Mansat-De Mas V, Ruidavets JB, Cariven P, Demur C, Payrastre B, Laurent G, Racaud-Sultan C. Expression of focal adhesion kinase in acute myeloid leukemia is associated with enhanced blast migration, increased cellularity, and poor prognosis. Cancer Res. 2004; 64:3191–3197. [PubMed: 15126359]

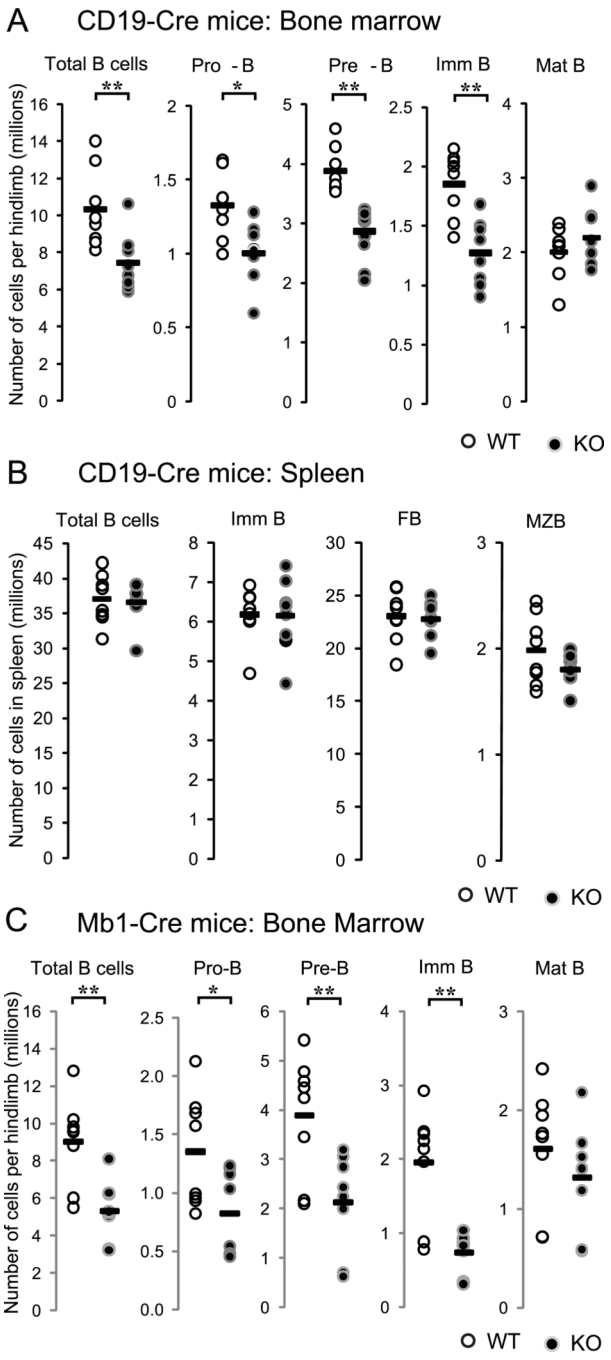

Figure 1. Selective decrease of progenitor B cell number in B cell specific FAK knockout mice

(A) BM cells from *Cd19-Cre Fak* KO or WT control mice, (B) spleen cells from *Cd19-Cre Fak* KO or WT control mice, or (C) BM cells from *mb1-Cre Fak* KO or littermate WT control mice were prepared and stained with monoclonal antibodies. Total numbers of each population per limb (one femur and one tibia) or per spleen were calculated using flow cytometry analysis and automated complete blood count. Student's t-tests were performed as shown *, $P<0.05$, and **, $P<0.01$ (unpaired, two-tailed). n=8. Dots indicate individual mice; bar indicates the mean. BM cell gates: Total B cells ($B220^+$ $CD19^+$), Pro-B ($B220^{lo}$ $CD19^+$ IgM^- $CD43^+$), Pre-B ($B220^{lo}$ $CD19^+$ IgM^- $CD43^-$), Imm B (immature B cells, $B220^{lo}$ $CD19^+$ IgM^+ $AA4.1^+$), Mat B (mature B cells, $B220^{hi}$ $CD19^+$ IgM^+ $AA4.1^-$); spleen cell

gates: Total B (CD19+), Imm B (immature B, $CD19^{+}$ $CD23^{-}$ $CD21/35^{-}$), FB (follicular B cells, $CD19^{+}$ $CD23^{+}$ $CD21/35^{mid}$), MZB (marginal zone B cells, $CD19^{+}$ $CD23^{-/lo}$ $CD21/35^{hi}$). Data are pooled from 4 independent experiments.

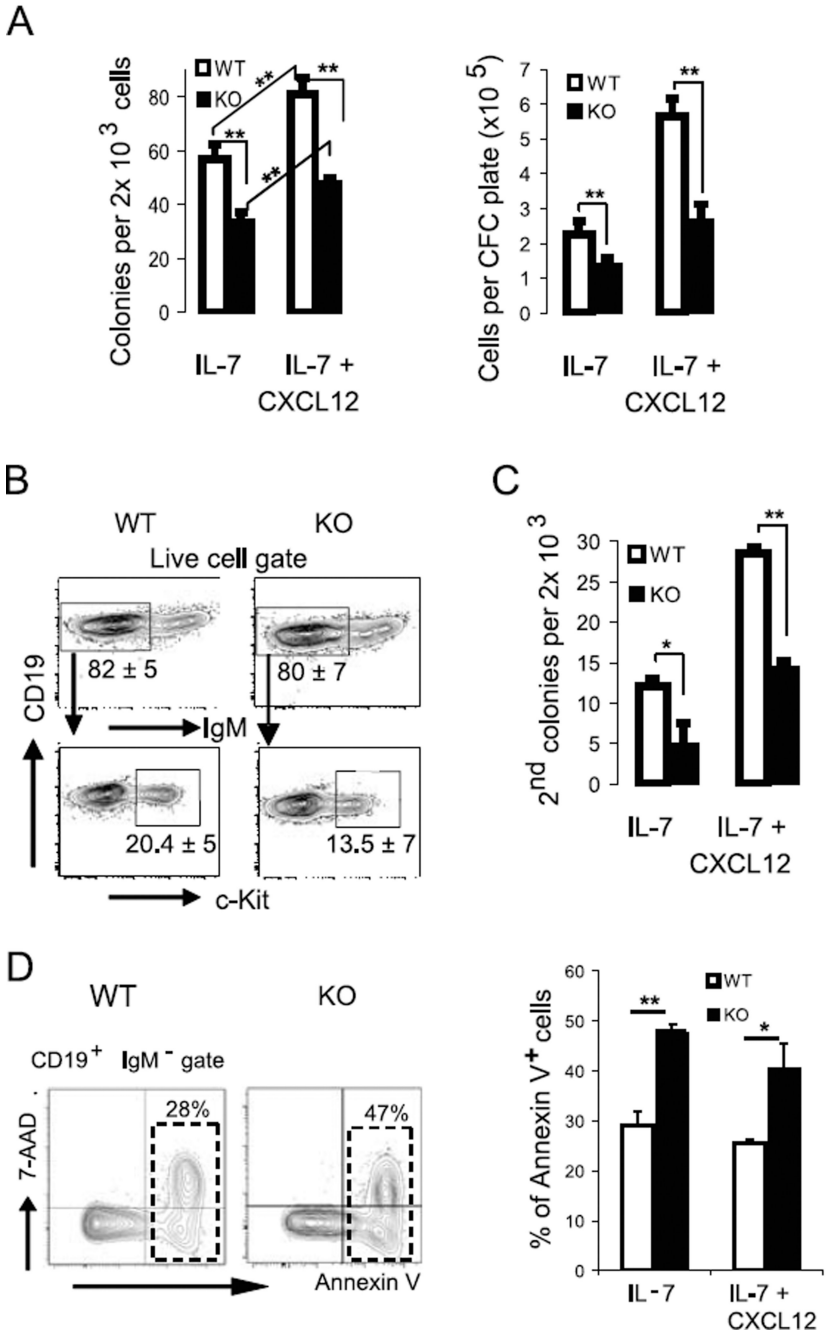

Figure 2. *Fak* deletion affects pro-B cell growth

(A – B) B220^{lo} IgM^{-} CD43^{+} EGFP^{+} sorted BM pro-B cells (2×10^{3} per plate) were sorted from CD19-*Cre*$^{+/-}$ *Fak*$^{fl/fl}$ Rosa26-EGFP$^{+/-}$ KO mice or WT mice, and plated in CFC pre-B (IL-7) media in the presence or absence of CXCL12 (500 ng/ml). (A) Colony count on day 7, followed by total live cell count after staining with 7-Aminoactinomycin D (7-AAD). (B) A representative flow cytometry analysis of 7-day CFC colonies is shown; % of IgM^{-} cells and IgM^{-} c-Kit^{+} cells is marked under each gate as mean ± standard error of the mean (SEM). Data are pooled from 10 experiments. (C) B220^{lo} IgM^{-} CD43^{+} EGFP^{+} BM cells (2×10^{3} per plate) were plated in CFC pre-B (IL-7) media in the presence or absence of CXCL12 (500 ng/ml). Colonies were recovered after 7 days and re-plated under the same

culture conditions (2×10^3 per plate). The number of secondary colonies was counted on day 7 (n=10). Data are pooled from 10 experiments. (D) Cells from the CFC colonies were analyzed by flow cytometry. The fraction of apoptotic (Annexin V^+ 7-AAD^-) and dead (Annexin V^+ 7-AAD^+) cells were assessed among the $CD19^+$ IgM^- cell population. % Annexin V^+ (apoptotic and dead) cells were plotted (mean ± SEM). Data are pooled from 4 experiments. Student's t-test, *P < 0.05, **P < 0.01.

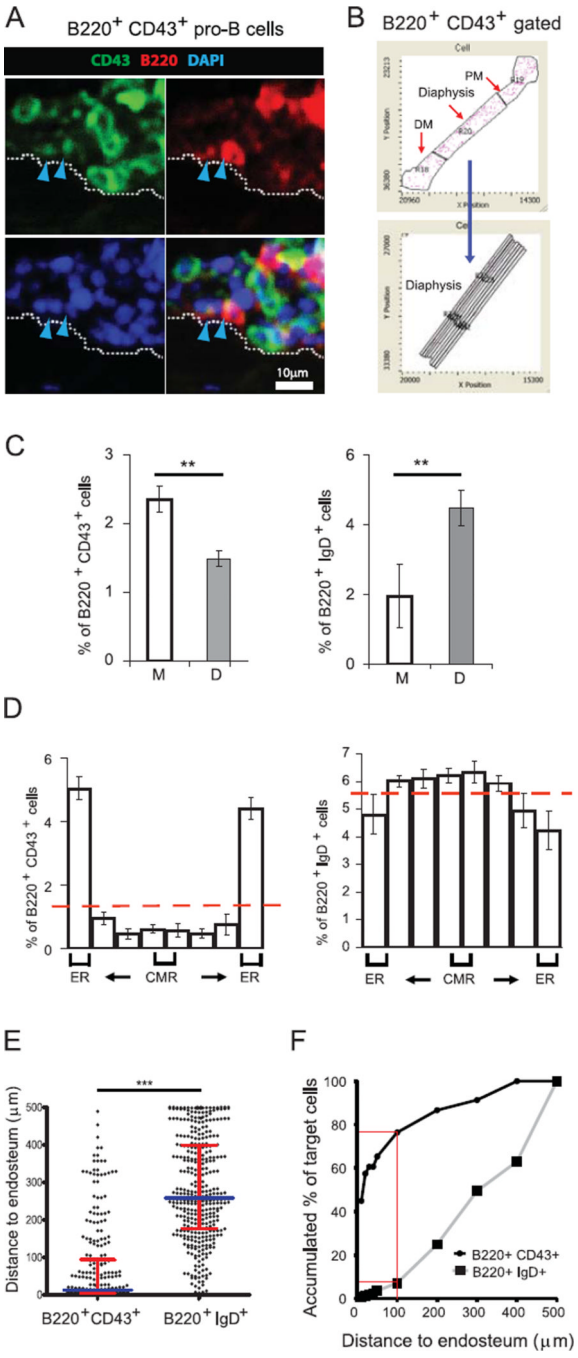

Figure 3. Non-random gradient distribution of B220$^+$ CD43$^+$ pro-B cells in the endosteal region of the metaphyses and the diaphysis

Longitudinal femur sections from C57BL/6 wild type (WT) mice were stained for B220 (red), CD43 or IgD (green), and DAPI (blue) followed by iCys imaging cytometry analysis. (A) Representative field images show BM cells on the endosteal surface (white dotted line). Arrowheads indicate B220$^+$ CD43$^+$ pro-B cell. (B) DAPI-based cell contour events retain their positional information so that the distribution of discrete cell populations, i.e. B220$^+$ IgD$^+$ cells and B220$^+$ CD43$^+$ cells, can be visualized in a tissue map with specific gates across the diaphysis within different regions (proximal and distal metaphysis, diaphysis, and subregions of the diaphysis). (C) Frequencies (mean ± SEM) of fluorescently stained B220$^+$

IgD^+ and $B220^+$ $CD43^+$ cell subpopulations within the metaphyses and diaphysis. Student's T-test, **P<0.01, n=4; NS, not significant. (D) The distribution of each population ($B220^+$ IgD^+ cells and $B220^+$ $CD43^+$ cells) is shown across the diaphysis. (ER=endosteal region; CMR=central medullary region). (E) The comparative distance of $B220^+$ $CD43^+$ cells and $B220^+$ IgD^+ cells to the bone surface in endosteal areas. Values plotted are values per cell. Scatter dot plots are shown with median ± interquartile range shown as broader and narrower horizontal lines, respectively. $n = 4$ mice. Two-tailed Mann-Whitney test: ***P < 0.0001. (F) Accumulated % of cells shows the preferential accumulation of $B220^+$ $CD43^+$ cells in endosteal areas compared to $B220^+$ IgD^+ cells. Red lines indicate the accumulated % of target cells within 100 μm distance to endosteum. Data are pooled from 4 independent experiments.

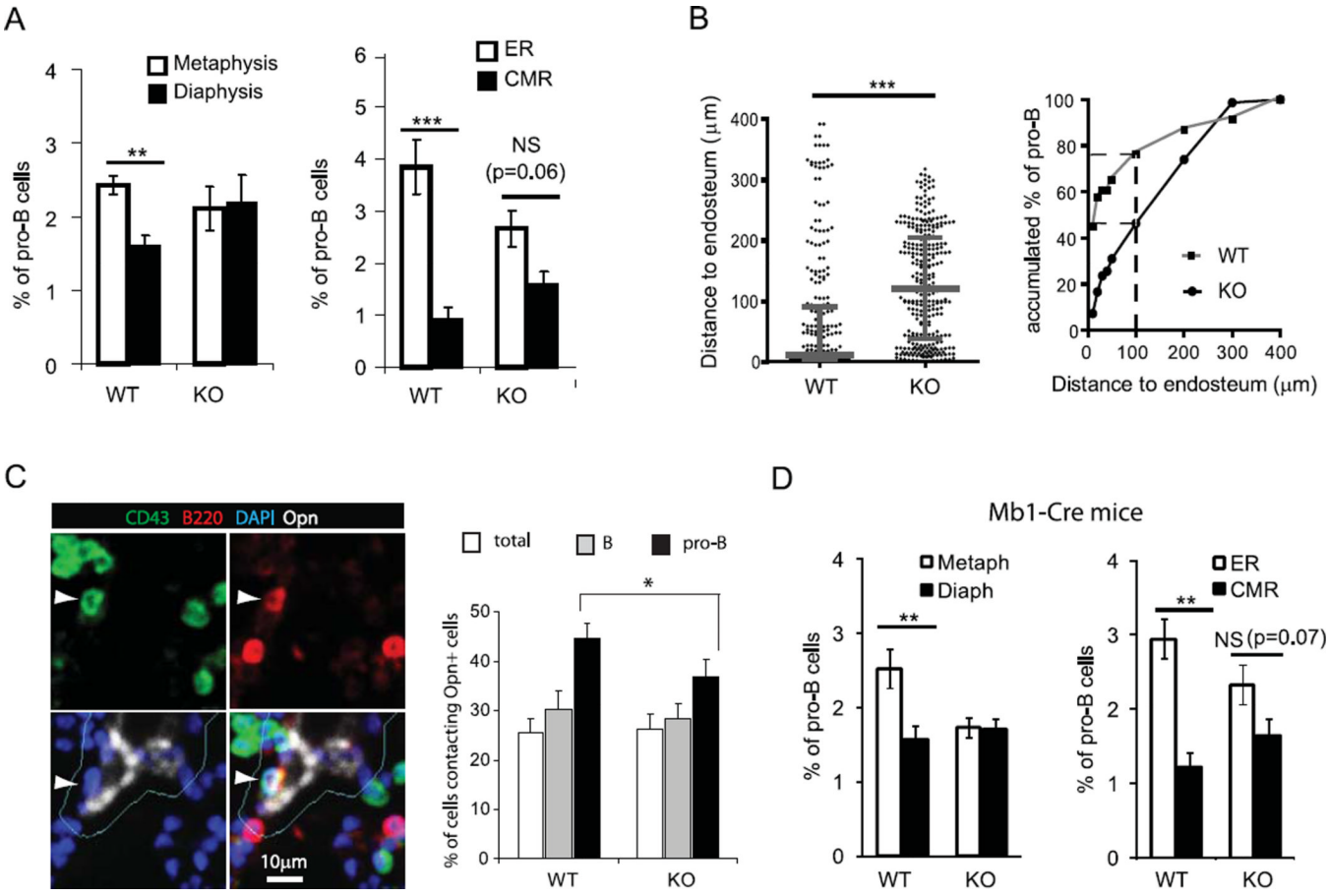

Figure 4. FAK regulates the distribution of pro-B cells in femoral BM microenvironments

Based on their frequency within specific BM regions of CD19-Cre *Fak* KO and WT control mice, $B220^+$ $CD43^+$ pro-B cells were graphed in the (A) metaphyses versus diaphysis of BM and in the ER (endosteal region) versus CMR (central medullary region) of diaphysis. Columns and error bars represent mean ± SEM. Student t-test: **, P<0.01; ***, P<0.001; NS, not significant. n=4. (B) The distances of CD19-Cre *Fak* KO and WT control $B220^+$ $CD43^+$ pro-B cells to endosteum in endosteal areas were measured and graphed ($n = 4$ mice). Dots indicate individual cells, n=262 (WT) and n=300 (KO). A scatter dot plot is shown with median ± interquartile range indicated as broader and narrower horizontal lines, respectively. Two-tailed Mann-Whitney test: ***P < 0.001. Accumulated % of $B220^+$ $CD43^+$ pro-B cells from WT or *Fak* KO mice is shown in endosteal areas. Numbers of cells analyzed for the Distance to endosteum, n=262 (WT) and n=300 (KO). Broken lines indicate the Accumulated % of target cells within 100 μm distance to endosteum. (C) Longitudinal femur sections were stained with antibodies against B220 (red), CD43 (green), and osteopontin (white), and DAPI (blue) followed by iCys imaging cytometry analysis. Representative field images show $B220^+$ $CD43^+$ pro-B cell (white arrowhead) on the $osteopontin^+$ niche. Cellular events in $osteopontin^+$ integration contour (within 5 μm outside of $osteopontin^+$ signals; Cyan) are identified as cells contacting Opn^+ cells. Percentages (mean ± SEM) of total cells, $B220^+$ B cells, and $B220^+$ $CD43^+$ pro-B cells contacting $osteopontin^+$ cells are shown in the metaphyses of CD19-Cre *Fak* WT and KO. Average of 39,683 (WT) and 38,354 (KO) cells in the metaphyses of femur sections were analyzed from 4 mice each. Student's t-test, *P<0.05, n=4. Data are pooled from 4 independent experiments. (D) The frequency of $B220^+$ $CD43^+$ pro-B cells within specific BM regions of

mb1-Cre *Fak* KO and WT control mice, were graphed in the metaphyses versus diaphysis of BM and in the ER (endosteal region) versus CMR (central medullary region) of diaphysis as shown in Fig. 4 (A). Student t-test: *, P<0.05; **, P<0.01; NS, not significant. n=3.

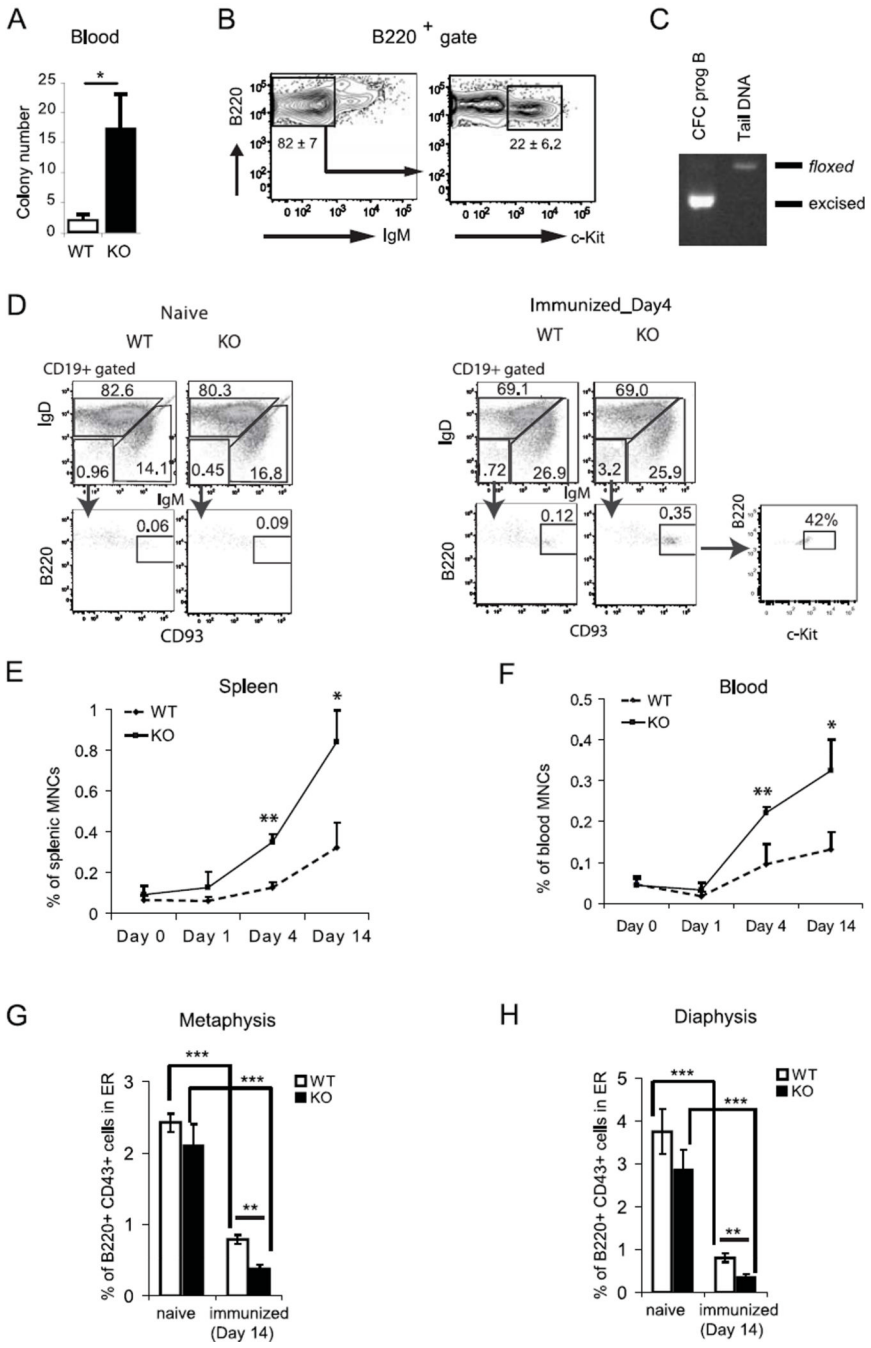

Figure 5. *Fak* deletion leads to mobilization of pro-B cells to the periphery

(A–C) Appearance of colony forming pro-B cells in the periphery of *Fak* KO mice under steady state condition. Representative data of four experiments are shown (n=8). (A) CFC assays were performed to detect pro-B cells from hemolyzed peripheral blood (0.25 ml per dish) in methylcellulose-based IL-7 containing CFC media. Colonies were counted on day 7 and plotted as colony number per 1 ml blood. Data are expressed as the mean ± SEM (n=12, *P<0.05). (B) Representative flow cytometry plot of $B220^+$ gated cells is shown. Mean percentages of $B220^+$ IgM^- and $B220^+$ IgM^- c-Kit^+ subpopulations are shown in the indicated gates. (C) The CFC cells from *Fak* KO mice were subjected to *Fak* genotyping as shown in Fig. S1. (D–F) Appearance of $B220^{lo}$ $CD19^+$ IgM^- IgD^- $CD93^+$ progenitor B cells

in the spleen and peripheral blood (PB) of immunized WT and *Fak* KO mice at days 0–14 were characterized and enumerated by flow cytometry (n=4). (D) Representative flow cytometry profiles of $B220^{lo}$ $CD19^{+}$ IgM^{-} IgD^{-} $CD93^{+}$ progenitor B cells in WT spleen from naïve and immunized on day 4 are shown. The frequencies of $CD93^{+}$ $B220^{lo}$ gated cells are indicated as % of total cells. The frequency of c-Kit^{+} progenitor B cells is indicated as % of $CD93^{+}$ $B220^{lo}$ cells. Kinetics of $B220^{lo}$ $CD19^{+}$ IgM^{-} IgD^{-} $CD93^{+}$ progenitor B cell numbers in spleen (E) and PB (F) after immunization. (G and H) Localization of $B220^{+}$ $CD43^{+}$ pro-B cells were examined in the BM from naïve and NPCGG/alum-immunized femurs (n=4) by LSC as described in Fig.4. The frequency of $B220^{+}$ $CD43^{+}$ pro-B cells in the endosteal region (within 100 μm distance endosteal surface) are graphed (G) in the metaphyses and (H) in the diaphysis. Data are from 4 independent experiments. Asterisks indicate significant differences from controls: *, $P < 0.05$; **, $P < 0.01$; ***, $P < 0.001$.

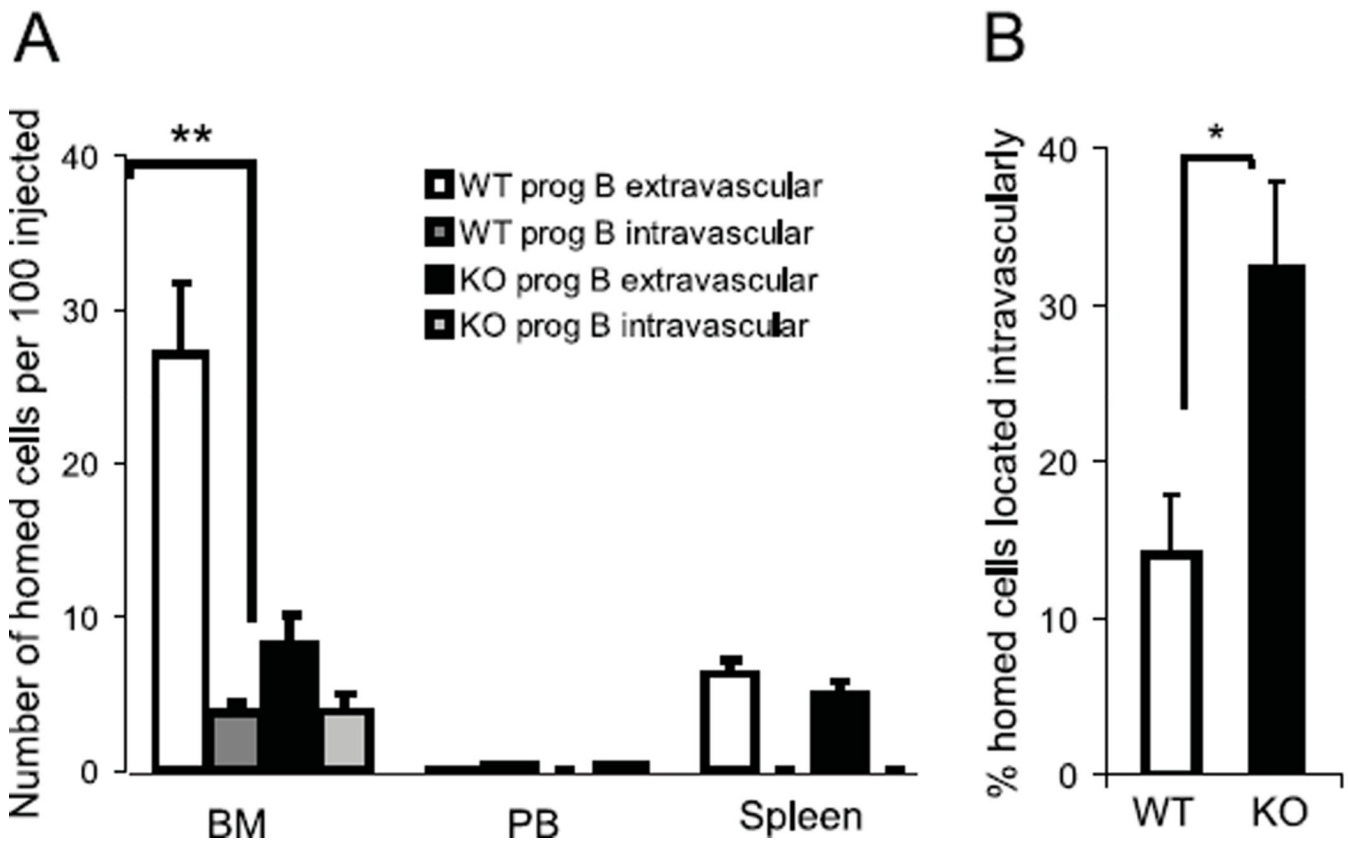

Figure 6. Pro-B cell homing to the BM cavity is regulated by FAK

Sorted B220^{+} CD43^{+} EGFP^{+} pro-B cells from *Fak* KO or WT were differentially labeled with CMFDA and CMAC dyes, respectively, and intravenously transferred to wild type recipient mice. After 2 hrs, intravascular cells were labeled *in vivo* by PE-Cy7 conjugated B220 antibodies and the frequency of total cells that homed to BM as well as the fraction present intravascularly was determined by FACS. (A) Homing abilities are expressed as the number of homed cells per 100 injected cells. Columns and error bars represent mean ± SEM. n=6, p=0.004 (Student's t-test). (B) The percentage of homed cells residing intravascularly is plotted for transferred WT and *Fak* KO cells. N=6, p=0.019 (Student's t-test). Data are from 3 independent experiments. *P<0.05, **P<0.01